Optimal Approach and Departure Trajectories with Acoustic Footprint Assessment for an Air Mobility Quad-Rotor

Varriale, Carmine; Yunus, F.; Snellen, M.

Publication date
2024

Document Version
Final published version

Published in
34th Congress of the International Council of the Aeronautical Sciences (ICAS)

OPTIMAL APPROACH AND DEPARTURE TRAJECTORIES WITH ACOUSTIC FOOTPRINT ASSESSMENT FOR AN AIR MOBILITY QUAD-ROTOR

Carmine Varriale[1,2], Furkat Yunus[1,3] & Mirjam Snellen[1,3]

[1]Delft University of Technology, Faculty of Aerospace Engineering
[2]Department of Flow Physics and Technology, Flight Performance and Propulsion section
[3]Department of Control and Operations, Aircraft Noise and Climate Effects section

Abstract

Advanced Air Mobility (AAM) vehicles are usually capable to operate in both forward and vertical flight thanks to their design configurations featuring multiple (tilting) rotors. Such maneuvering agility can be leveraged to minimize their acoustic footprint during operations close to the ground. The present work compares the acoustic footprint of optimal trajectories of AAM aircraft using low-order aero-acoustic models. The methodology is applied to the case of an AAM quad-rotor aircraft, which is modelled as a rotating point-mass with three Degrees of Freedom and two input controls. The trajectories are globally optimal in the sense of standard mission objectives, such as maneuver time or traveled horizontal distance, and are subject to realistic performance constraints. Results show that minimum-time trajectories generate higher and more concentrated noise footprints compared to minimum-distance trajectories, which distribute noise levels more evenly and result in overall lower noise footprints. Departure trajectories exhibit lower noise levels than approach trajectories. Adopting minimum-distance trajectories can significantly reduce noise impacts for both approach and departure maneuvers.

Keywords: trajectory optimization, optimal control, acoustic footprint, noise impact, advanced air mobility

Nomenclature

$\mathbf{b}$	non-linear terminal constraints	D	drag force, N
$\mathbf{f}$	dynamic equations	I_y	lateral inertia, $\mathrm{kg\,m^2}$
$\mathbf{g}$	path inequality constraints	J	cost functional
$\bar{c}$	blade mean aerodynamic chord, m	L	Lagrange's running cost
h	altitude, m	P	power required, W
m	mass, kg	R	rotor radius, m
q	pitch rate, rad/s	T_i	thrust of rotor i, N
t	time, s	V	airspeed, m/s
u	longitudinal velocity, m/s	W	weight, N
$\mathbf{u}$	control vector	α_f	fuselage angle of attack, rad
w	normal velocity, m/s	ξ	flight path angle, rad
w_in	induced velocity, m/s	ρ	air density, $\mathrm{kg/m^3}$
x_E	horizontal position in Earth axes, m	σ	rotor solidity
x_{T_i}	position of rotor i in body axes, m	$\theta_{0.75}$	collective angle, rad
$\mathbf{x}$	state vector	θ_f	fuselage pitch angle, rad
A_{eq}	equivalent skin-friction area, $\mathrm{m^2}$	θ_tw	non-dimensional twist gradient, rad
C_d	drag coefficient	Ω	rotor angular velocity, rad/s
C_{l_α}	two-dimensional lift curve slope, 1/rad	Ψ	Mayer's terminal cost

1. Introduction

Considerable attention has been recently dedicated to the minimization of noise footprint due to aerial operations. In these regards, many approaches have been proposed to optimize the trajectory of conventional helicopters during approach or departure maneuvers. On the basis of the application and motivation, the models employed span across a wide range of complexities and fidelities, both for the flight mechanics and the aero-acoustic analyses.

A method to minimize the noise footprint of helicopters during simultaneous non-interfering approaches has been proposed in [1]. The helicopter is regarded as a point mass with three translational Degrees of Freedom (DoFs), and metrics such as the number of awakenings and noise level contours on the ground have been used to estimate the noise impact. A similar approach is adopted in [2], where rotational DoFs and directional dynamics are also included. Noise impact is calculated by combining a noise source model (function of flight path and roll angles) and an atmospheric attenuation model, and synthesized in a surrogate model for trajectory optimization. Optimal helicopter trajectories are obtained in [3, 4] for complex atmospheric conditions and subject to realistic geographical constraints. The helicopter is modeled as a non-rigid system with eight DoFs, and the noise footprint is estimated using models for noise generation, propagation and impact.

With the advent of Advanced Air Mobility (AAM), different vehicle configurations have become objects of interest from both a flight mechanics and aero-acoustic perspective. This is especially in light of their ability to operate both in forward and vertical flight. A methodology to estimate the acoustic impact of an AAM vehicle in operational trajectories is presented in [5] for an approach maneuver over a flat terrain. The noise footprint is calculated using high-fidelity Computational Fluid Dynamics (CFD) simulations, and a surrogate model is created to be used during flight mechanics simulations. The trajectories are imposed a priori, and the aircraft is modeled as a multi-body system with four effective DoFs (two of which pre-determined by the trajectory). Trajectory optimization of multi-rotor aircraft, especially regarding operational scenarios, is expected to become a relevant topic in the near future. The higher number of rotors, together with the complex aero-acoustic interaction among them, makes the noise footprint calculation much more computationally expensive, and also more necessary.

Noise source models for propeller- or rotor-driven aircraft are typically calculated using high-fidelity CFD simulations combined with the Ffowcs Williams and Hawkings (FW-H) acoustic analogy. However, the computational demands of this method make it impractical to assess the noise footprint of an entire flight trajectory. Even more so, integrating aero-acoustic simulations into an aircraft design optimization loop to explore the include considerations on the impact of design parameters becomes on the noise footprint becomes completely unfeasible. In contrast, recent works emphasize low-order approaches as a practical solution for evaluating flight trajectory noise footprints [6, 7]. These approaches utilize an aerodynamic model, an aero-acoustic model, and a propagation model. Focused specifically on propellers/rotors as the primary noise source, low-order methods stand out for their computational efficiency and reliability.

This paper compares the acoustic footprint of optimal approach and departure trajectories of an AAM quad-rotor aircraft using low-order aero-acoustic models. The methodology used to calculate the optimal trajectories and the noise footprint is presented in Section 2. Section 3.describes the aircraft model and the scenarios that are going to be simulated, and Section 4. presents the preliminary results obtained. Finally, Section 5.draws some preliminary conclusions and outlines the envisioned steps for future work.

2. Methodology

The proposed methodology is composed of two phases. The first phase consists in calculating the optimal trajectories of the vehicle starting from a high-level description of the desired maneuvers. The second phase consists in calculating the acoustic footprint resulting from such maneuvers. The following sections describe the models and methods in more detail.

2.1 Flight Mechanics model

The aircraft is modeled as a rigid system with three DoFs in a vertical plane: horizontal and vertical translations, and rotation about its pitch axis. Earth is assumed flat, with a constant acceleration of

gravity g, standard atmosphere and no wind. The aircraft dynamic evolution $\mathbf{f}(\mathbf{x},\mathbf{u},t)$ is described by the following set of ordinary differential equations in body axes (origin at the aircraft center of gravity, x-axis towards the aircraft nose, z-axis oriented as the pilot head-to-feet direction):

$$m(\dot{u}+qw) = -W\sin\theta_{\mathrm{f}} - D\cos\alpha_{\mathrm{f}} \tag{1}$$
$$m(\dot{w}-qu) = W\cos\theta_{\mathrm{f}} - D\sin\alpha_{\mathrm{f}} - \textstyle\sum_i T_i \tag{2}$$
$$I_y\dot{q} = \textstyle\sum_i T_i x_{T_i} \tag{3}$$
$$\dot{x}_E = V\cos\xi \tag{4}$$
$$\dot{h} = V\sin\xi \tag{5}$$
$$\dot{\theta}_{\mathrm{f}} = q \tag{6}$$

The flight path angle ξ is positive for climbing flight. The angle of attack α_f is positive if the airspeed vector impinges on the lower side of the fuselage, and is calculated as in Eq. 7 using the MATLAB-based four-quadrant inverse tangent[1]. This choice allows to obtain $\alpha_{\mathrm{f}} = 0$ in case both $u = 0$ and $w = 0$, as it happens in hover.

$$\alpha_f = \arctan_{4\mathrm{Q}}(w/u) \tag{7}$$

The airspeed V is calculated as in Eq. 8.

$$V = \sqrt{u^2+w^2} \tag{8}$$

Aerodynamic drag D due to the aircraft fuselage is expressed in terms of dynamic pressure and equivalent skin-friction area according to Eq. 9. Aerodynamic lift due to the aircraft body is neglected for simplicity.

$$D = \rho V^2 A_{eq}/2 \tag{9}$$

All rotors are assumed to be rigid and operating at the same rotational speed Ω, which is held constant throughout the maneuver, in a similar way as done in [5]. The thrust produced by each rotor is assumed to be orthogonal to the rotor plane, hence parallel to the aircraft z body axis. Thrust is expressed in terms of a thrust coefficient C_T according to Eq. 10, and its magnitude is controlled by a collective command $\theta_{0.75}$ which is measured with respect to the blade at the 75% radius station.

$$T_i = \pi\rho\Omega^2 R^4 C_{T_i}(\theta_{0.75}) \tag{10}$$

The induced velocity w_{in} at each rotor is estimated using Glauert's formula, reported in Eq. 11 [8]. This approach assumes that the inflow adapts instantaneously to the change of rotor thrust, and therefore neglects any inflow dynamics.

$$w_{\mathrm{in}}:\ C_T = 2w_{\mathrm{in}}\sqrt{u^2+(w+w_{\mathrm{in}})^2}/(\Omega R)^2 \tag{11}$$

Such induced velocity is then used to estimate the power coefficient C_{P_i} required by each rotor, which is expressed as in Eq. 12 using the integral results of Blade Element Momentum Theory (BEMT) [8].

$$C_P = C_T\sqrt{\frac{C_T}{2}}\left(\frac{K_{\mathrm{in}}w_{\mathrm{in}}+w}{\Omega R}\right) + \frac{\sigma C_d}{8}\left[1+4.65\left(\frac{u}{\Omega R}\right)^2\right] \tag{12}$$

The total power P required by the aircraft is then calculated as in Eq. 13.

$$P = DV + \sum_i \pi\rho\Omega^3 R^5 C_{P_i} \tag{13}$$

The collective angle $\theta_{0.75}$ resulting in the calculated combination of thrust coefficient and inflow velocity is estimated using Eq. 14, which is valid for rotors with constant chord and linear twist distributions along the radius [8].

$$\theta_{0.75}:\ C_T = \frac{C_{l_\alpha}\sigma}{2}\left\{\frac{\theta_{0.75}}{3}\left[1+\frac{3}{2}\left(\frac{u}{\Omega R}\right)^2\right] + \frac{\theta_{\mathrm{tw}}}{4}\left[\left(\frac{u}{\Omega R}\right)^2+1\right] - \frac{1}{2}\left(\frac{w+w_{\mathrm{in}}}{\Omega R}\right)\right\} \tag{14}$$

[1] Documentation: `https://nl.mathworks.com/help/matlab/ref/atan2.html`. Accessed on: June 15, 2024.

2.2 Trajectory optimization

Optimal trajectories are calculated using the formalism of optimal control theory [9–11]. Solving an optimal control problem means obtaining the time histories of the states $\mathbf{x}(t)$ and control inputs $\mathbf{u}(t)$ that minimize an assigned cost functional $J(t,\mathbf{x},\mathbf{u})$, while complying to a set of kinematic, dynamic, and performance constraints. The optimal control problem is formulated as in Eq. 15,

$$\begin{aligned}
\min_{\mathbf{x},\mathbf{u}} \quad & J = \Psi(\mathbf{x}(t_f),t_f) + \int_{t_0}^{t_f} L(\mathbf{x}(t),\mathbf{u}(t),t)\,\mathrm{d}t \\
\text{s.t.} \quad & \dot{\mathbf{x}}(t) = \mathbf{f}(\mathbf{x}(t),\mathbf{u}(t),t) \\
& \mathbf{g}_{\min} \leq \mathbf{g}(\mathbf{x}(t),\mathbf{u}(t),t) \leq \mathbf{g}_{\max} \\
& \mathbf{x}_{\min} \leq \mathbf{x}(t) \leq \mathbf{x}_{\max} \\
& \mathbf{u}_{\min} \leq \mathbf{u}(t) \leq \mathbf{u}_{\max} \\
& \mathbf{b}(\mathbf{x}(t_f),\mathbf{u}(t_f),t_f) = \mathbf{b}_f \\
& \mathbf{x}(t_0) = \mathbf{x}_0 \\
& \mathbf{x}_{f,\min} \leq \mathbf{x}(t_f) \leq \mathbf{x}_{f,\max}
\end{aligned} \tag{15}$$

where $\mathbf{x}_0$ and $\mathbf{x}_f$ are assigned initial and final conditions on the states.
Because of the symmetry of the problem, it is assumed that the two front rotors operate at the same thrust coefficient, and the same is true for the pair of rear rotors. Therefore, the two thrust coefficients C_T^{fr} and C_T^{re} are sufficient to control the motion of the aircraft. To avoid incurring in excessively high control input rates — which may result in detrimental fluctuations of the states, with consequent sub-optimal performance and/or slow convergence of the solver — the flight mechanics model and the optimal control problem formulation are augmented using the following procedure, sometimes referred to as "input damping" [3]:

- two trivial equations are added to Eqs. 1–6 to capture the rate of change of the thrust coefficients, as shown in Eq. 16;

$$\begin{aligned}
\dot{C}_T^{\mathrm{fr}} &= C_T^{\mathrm{fr}} \\
\dot{C}_T^{\mathrm{re}} &= C_T^{\mathrm{re}}
\end{aligned} \tag{16}$$

- the latter rates are chosen as the components of the control vector $\mathbf{u}$;
- a penalization term J_{pen} is added to the cost functional J to minimize the variation of thrust coefficients over time:

$$J_{\mathrm{pen}} = \lambda \int_{t_0}^{t_f} \left(\dot{C}_T^{\mathrm{fr}} + \dot{C}_T^{\mathrm{re}}\right)^2 \mathrm{d}t \tag{17}$$

  where λ is a scaling factor that can be assigned on the basis of the application.

The overall state and control vectors are therefore defined as in the following Eq. 18.

$$\begin{aligned}
\mathbf{x} &= \begin{bmatrix} u & w & q & x_E & h & \theta_{\mathrm{f}} & C_T^{\mathrm{fr}} & C_T^{\mathrm{re}} \end{bmatrix}^\top \\
\mathbf{u} &= \begin{bmatrix} \dot{C}_T^{\mathrm{fr}} & \dot{C}_T^{\mathrm{re}} \end{bmatrix}^\top
\end{aligned} \tag{18}$$

The optimal trajectory is subject to the following set of path inequality constraints $\mathbf{g}$, which ensures that the aircraft flies forward or vertically (never backwards), follows a continuous climb or descent path, and never exceeds the power made available by the engine.

$$\mathbf{g} = \begin{Bmatrix} V\cos\xi \\ V\sin\xi \\ P/P_{\max} \end{Bmatrix} \in \begin{Bmatrix} [0,+\infty) \\ [0,+\infty) \text{ or } (-\infty,0] \\ [0,1] \end{Bmatrix} \tag{19}$$

The initial time instant t_0 is always assumed to be zero, and the final time instant t_f is always left free to be determined by the optimizer. The terminal constraints $\mathbf{b}$ are used to ensure that the aircraft

ends the maneuver in the steady state. Namely:

$$\mathbf{b} = \begin{Bmatrix} \dot{u} \\ \dot{w} \\ \dot{q} \end{Bmatrix} = \begin{Bmatrix} 0 \\ 0 \\ 0 \end{Bmatrix} \tag{20}$$

The ICLOCS2[2] open-source toolbox is used to transcribe the optimal control problem into a large sparse Non-Linear Programming (NLP) problem. The latter is solved by using direct collocation with Hermite-Simpson discretization, as each trajectory consists of only one phase and is expected to be relatively smooth [12]. The numerical optimization is carried out with the open-source solver IPOPT[3] (Interior Point OPTimizer) [13, 14], which uses an interior point line search filter method.
The trajectories obtained with this methodology are then sampled approximately every $0.5\,\mathrm{s}$ in order to perform the acoustic analysis described in the following section. The number of samples for each trajectory is equal to $N = \lfloor (t_f - t_0)/0.5\,\mathrm{s} \rfloor$.

2.3 Acoustic footprint

The computation of the acoustic footprint involves three distinct steps: aerodynamic calculation, aero-acoustic calculation, and noise footprint prediction. The aerodynamic model relies on the Blade Element Momentum Theory (BEMT) and assumes a uniform inflow condition. Flight parameters, such as vehicle speed, pitch angle, rotational speed, and collective pitch, extracted from the flight trajectory are used at each sampled instant to calculate aerodynamic forces (sectional thrust and torque distribution along the blade's radial direction) responsible for noise generation. Additional details can be found in [7, 15].
The aero-acoustic solver is based on Hanson's frequency-domain acoustic formulation for steady loading and thickness noise, incorporating non-compactness, sweep, and non-axial ($\alpha_\mathrm{f} \neq 0$) flow effects [16–19]. Stationary loading noise calculation involves using sectional thrust and torque derived from the aerodynamic model, while thickness noise is determined using blade geometry. Further information on this process can be accessed in the solver's input file description provided in [19]. Validation against high-fidelity CFD simulation results, time-domain compact dipole/monopole FW-H formulation, and outdoor experimental measurements is discussed in [6, 15]. The aero-acoustic solver focuses solely on tonal noise resulting from steady loading on the blade and volume displacement caused by blade motion. In upcoming iterations, the solver will be enhanced to include broadband noise attributed to turbulent boundary layer trailing edge noise.
Individual rotor noise is computed first, and the overall noise from all rotors is determined by summing their contributions incoherently on microphones distributed over a noise sphere surrounding the vehicle. This noise sphere is then used as input for the propagation and footprint calculation module. The noise propagation and footprint calculation solver utilizes the $\mathrm{Opty}\partial\mathrm{B\_footprint}$ tool [5, 20] to propagate noise signals sampled on the noise source sphere to the ground receiver by employing the Noise Hemisphere Database (NHD) approach [5]. This consists in calculating narrow-band noise spectra corresponding to each flight and operating condition along the trajectory, and storing them in the NHD. To determine the noise footprint of a given trajectory, the source emission-time position for each ground microphone is first determined. Then, the corresponding noise sphere at each source emission position is retrieved from the NHD. If the corresponding noise sphere is not present in the database, it is interpolated from the three nearest conditions. Subsequently, narrow-band noise signals are propagated to the ground microphone using a ray-tracing propagation model. This model accounts for ground reflection under the assumption of a flat terrain and considers the influences of wind and temperature on noise propagation, as described in [20].

3. Application

The methodology presented in the previous section is applied to the case of an AAM quad-rotor aircraft. The vehicle and the simulated maneuvers are presented in this section.

[2] http://www.ee.ic.ac.uk/ICLOCS/Overview.html
[3] https://coin-or.github.io/Ipopt/

3.1 Aircraft model

The aircraft model under consideration is the single-passenger quad-rotor shown in Figure 1. Its design has been conceptualized for air-taxi operations in [21], considering different energy sources and power train configurations. The electric variant is chosen for the present analysis. This variant is expected to have flapping rotors operated at a constant rotational speed and controlled by means of a collective command, as this is deemed sufficient to guarantee attitude and flight path control to the aircraft. The addition of a cyclic command is suggested as a possibility to improve the aircraft maneuverability. Similar design concepts have been proposed in [7, 22, 23]. A comprehensive review of the state of the art on aircraft design concepts for AAM operations is presented in [24].
In the present work, the aircraft is considered as a single rigid body with constant mass and lateral inertia, hence neglecting the flapping and tilting motion of the rotors. A mean chord and a linear approximation of the twist distribution of the original geometry of the rotor presented in [25] have been used. The most relevant aircraft and rotor parameters are reported in Tables 1 and 2.

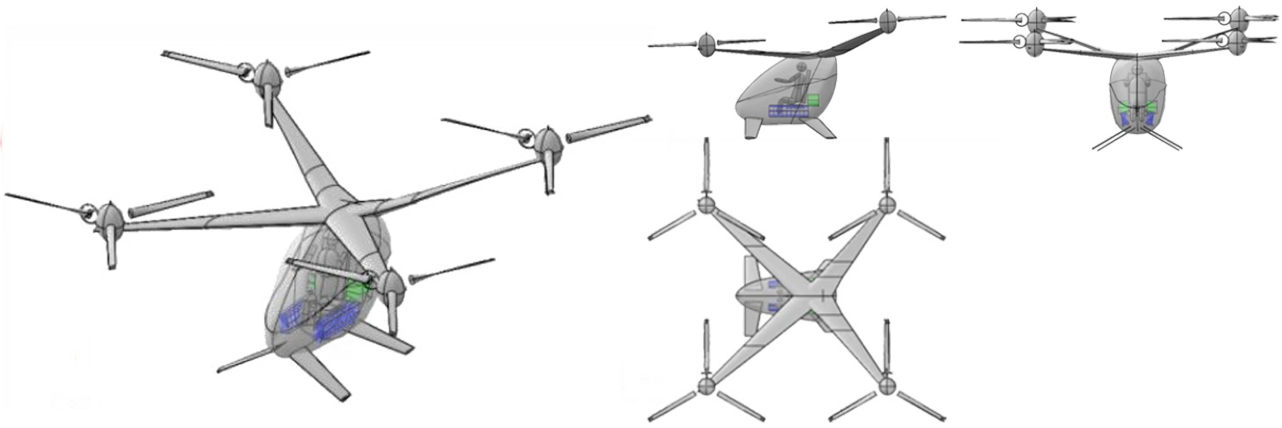

Figure 1 – Single-passenger electric quad-rotor aircraft concept [21]

Table 1 – Aircraft and rotor geometric parameters, extracted or estimated from [21, 25]

	m	I_y	R	A_{eq}	σ	$\bar{c}$	θ_0	θ_{tw}	$x_{T_{\text{fr}}}$	$x_{T_{\text{re}}}$	$z_{T_{\text{fr}}}$	$z_{T_{\text{re}}}$
Value	455	1600	1.92	0.32	0.145	0.291	48.0	-41.5	2.39	-2.79	-1.73	-2.40
Unit	kg	$\text{kg}\,\text{m}^2$	m	m^2	-	m	deg	deg/m	m	m	m	m

Table 2 – Aircraft and rotor performance parameters, extracted or estimated from [21, 25]

	V_{cr}	Ω	C_{l_α}	C_d	K_{in}	$C_{T_{\text{max}}}$	P_{max}
Value	36.5	716	0.104	128	1.15	$3.17 \cdot 10^{-2}$	64400
Unit	m/s	rpm	1/deg	counts	-	-	W

3.2 Maneuvers

Two sets of maneuvers are going to be analyzed in this work: one set for the approach phase from cruise to hover, and one set for the departure phase from hover to cruise. Each maneuver is performed using three different optimality criteria: minimum time, minimum horizontal distance, and minimum energy. This is in order to highlight the effect of the piloting strategy on the resulting noise footprint. The intention is to study the correlation between the aircraft acoustic footprint and the aircraft attitude during accelerated flight in proximity of the ground, in an abstract operational scenario. This is particularly relevant for a vehicle like a multi-rotor, which is capable to fly in both forward and vertical flight, and hence can have some degree of control on its noise directivity. The assigned maneuver parameters are reported in Table 3.

Table 3 – Maneuver parameters

Maneuver	Objective	Ψ	L	λ	$x_{E,0}$ (m)	$x_{E,f}$ (m)	h_0 (m)	h_f (m)	V_0 (m/s)	V_f (m/s)
Approach	Min. time	t_f	0	t_f	Free	0	200	5	36.5	0
	Min. distance	$\lvert x_{E,f}\rvert$	0	$\lvert x_{E,f}\rvert$	Free	0	200	5	36.5	0
	Min. energy	0	$P/P_{\max}$	1	Free	0	200	5	36.5	0
Departure	Min. time	t_f	0	t_f	0	Free	5	200	0	36.5
	Min. distance	$\lvert x_{E,f}\rvert$	0	$\lvert x_{E,f}\rvert$	0	Free	5	200	0	36.5
	Min. energy	0	$P/P_{\max}$	1	0	Free	5	200	0	36.5

In all cases, the aircraft flies in the positive direction of the x_E axis. The approach trajectories start in cruise conditions at $x_E < 0$, and end at $x_E = 0$ in hover conditions. The departure trajectories start in hover conditions at $x_E = 0$ and end at cruise conditions at $x_E > 0$.
Steady state conditions are imposed at both the initial and final instant of each maneuver. The corresponding flight parameters are found by trimming the aircraft for cruise or hover using Eqs. 21. These are obtained by imposing $\dot{u} = \dot{w} = \dot{q} = q = \xi = 0$ in Eqs. 1-3.

$$\theta_{\mathrm{f}} = \arctan\left(-\frac{D}{W}\right) \quad \Rightarrow \quad T_{\mathrm{fr}} = \frac{W\cos\theta_{\mathrm{f}} - D\sin\theta_{\mathrm{f}}}{1 - x_{T_{\mathrm{fr}}}/x_{T_{\mathrm{re}}}} \quad \Rightarrow \quad T_{\mathrm{re}} = -T_{\mathrm{fr}}\frac{x_{T_{\mathrm{fr}}}}{x_{T_{\mathrm{re}}}} \tag{21}$$

The bounding values for the state and control variables are reported in Table 4.

Table 4 – State and control bounds

	u	w	q	h	θ_{f}	C_T^{fr}	C_T^{re}	$\dot{C}_T^{\mathrm{fr}}$	$\dot{C}_T^{\mathrm{fr}}$
Lower bound	-40	-40	-10	5	-15	0	0	$-5\cdot10^{-4}$	$-5\cdot10^{-4}$
Upper bound	40	40	10	200	15	$C_{T_{\max}}$	$C_{T_{\max}}$	$5\cdot10^{-4}$	$5\cdot10^{-4}$
Unit	m/s	m/s	deg/s	m	deg	–	–	1/s	1/s

It is imagined that the hover condition occurs precisely above a landing pad, and therefore precedes the vertical descent necessary to touch down. The vertiport landing pad is located at $x_E = 0\,\mathrm{m}$ and $h = 0.8\,\mathrm{m}$ to comply with FAA regulations. The terrain is assumed flat and without any features in order to draw conclusions based exclusively on the aircraft performance.

4. Results

4.1 Trajectories

The optimal trajectories obtained for the scenarios described in the previous sections are reported in Figure 2 in the form of time histories of the most relevant flight parameters, for both approach and departure maneuvers. The approach trajectories for minimum distance and minimum time are referred to as AD and AT, respectively. Departure trajectories for minimum distance and minimum time are referred to as DD and DT, respectively. Trajectories for minimum energy coincide with those for minimum time, and therefore are not shown.
The AT maneuver is executed by continuously decelerating and descending until hover, while the AD maneuver is obtained with a deceleration at constant altitude until hover, followed by a vertical descent. In both cases, the aircraft loses altitude and/or airspeed by pitching its nose up to the allowed limit angle. Similar considerations are valid for the counterpart departure maneuvers, in reverse order. The DT maneuver consists in a continuous acceleration accompanied by a gradual increase of altitude. The DD maneuver is instead performed with a vertical ascent up to cruise altitude, followed by a transition to forward flight. In both cases, the aircraft gains forward speed and/or altitude by pitching its nose down to the allowed limit angle. For all maneuvers, the front rotors are always operating at a slightly higher thrust coefficient than the rear rotors, in light of the fact that

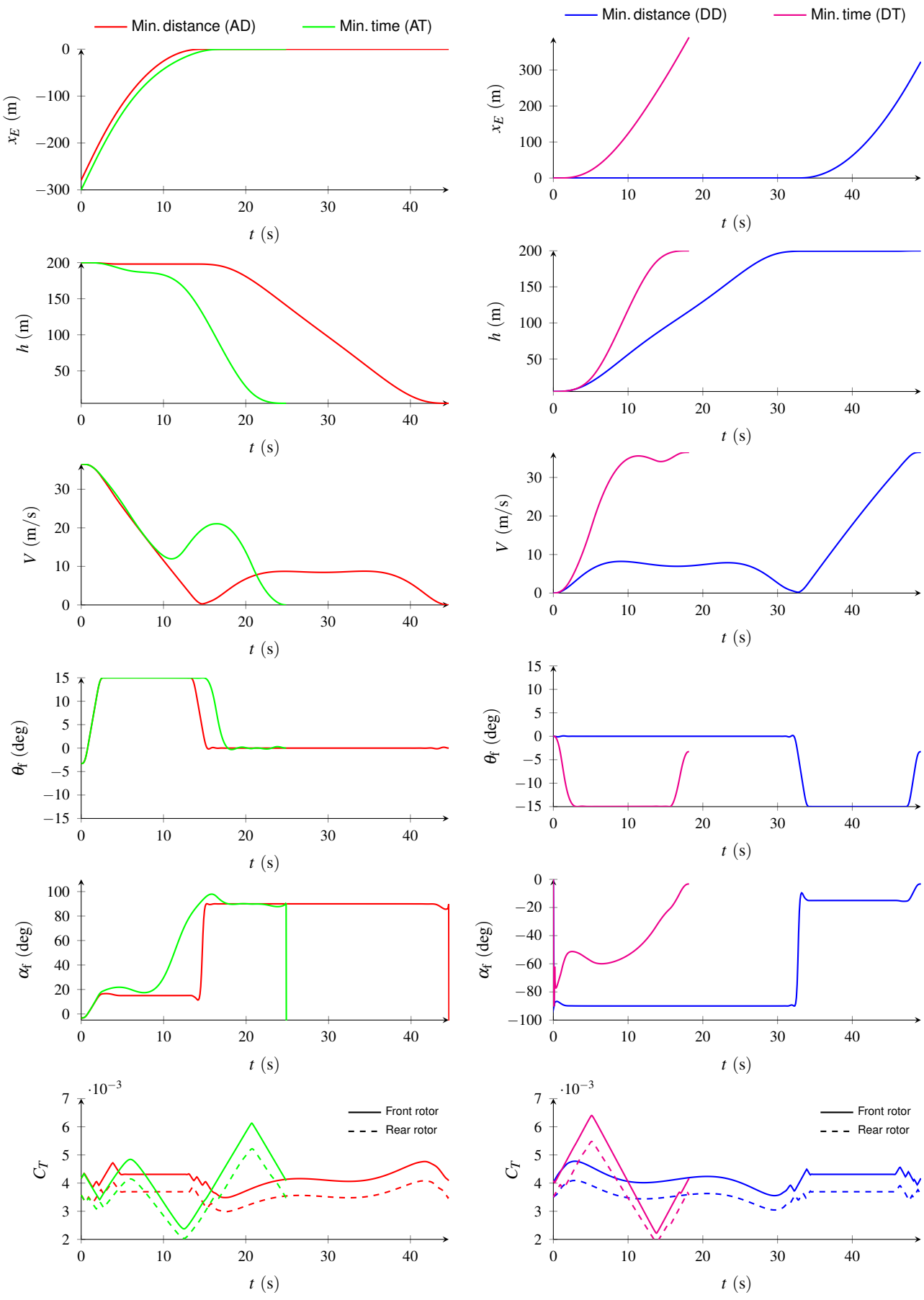

(a) Approach maneuvers

(b) Departure maneuvers

Figure 2 – Time histories of flight parameters during optimal trajectories

the former are closer to the center of gravity of the aircraft. Minimum-time trajectories are obtained with more aggressive collective controls, which are representative of a rate-limited bang-bang control strategy. The angle of attack of the fuselage reaches very high values during the transition to/from hover for both the minimum-time approach and departure trajectories, while its value stays reasonably contained for the horizontal flight phase of both the minimum-distance trajectories.

4.2 Effective Perceived Noise Levels

Acoustic footprints are computed for all the trajectories in terms of Effective Perceived Noise Levels (EPNLs). The EPNLs measure the overall perceived annoyance from aircraft noise considering duration and tonal corrections of the acoustic signal. Virtual receivers are distributed over flat terrain at the corners of a $5\,\mathrm{m} \times 500\,\mathrm{m}$ mesh grid, with an elevation of $1.2\,\mathrm{m}$. Only tonal noise up to the 10th harmonic of the Blade Passing Frequency (BPF) is considered in this study. It is important to note that the aerodynamic solver assumes a uniform inflow condition, and the acoustic solver does not account for broadband noise computation. As a result, the source directivity may not accurately capture the correct radiation pattern of the noise source during maneuvers.

As shown in Fig. 3, the AD and AT trajectories exhibit similar trends, with trajectory AT showing higher noise levels on the left half of the domain, and lower noise levels on the right half of it. This pattern is attributed to differences in flight speed and total duration of the trajectories. For trajectory AD, the vehicle approaches the vertiport by decelerating to zero speed at cruise altitude, and then descending slowly over approximately $25\,\mathrm{s}$. In contrast, trajectory AT involves significantly higher airspeed during the continuous descent and pitch rotation, which results in completing the landing in about $10\,\mathrm{s}$. Consequently, due to the higher approach speed and faster landing of trajectory AT near the vertiport, higher noise levels are generated on the left half of the terrain compared to those produced by trajectory AD. Similar trends have been noted in other studies, where it has been observed that higher flight speeds increase on-ground noise levels, making them undesirable during approach maneuvers [7, 26].

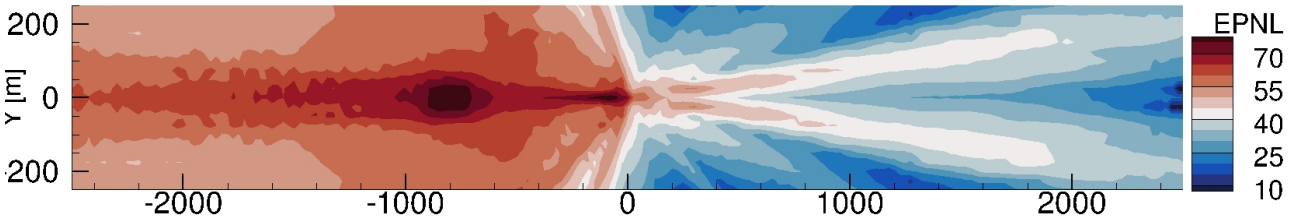

(a) Approach maneuver for minimum distance (AD)

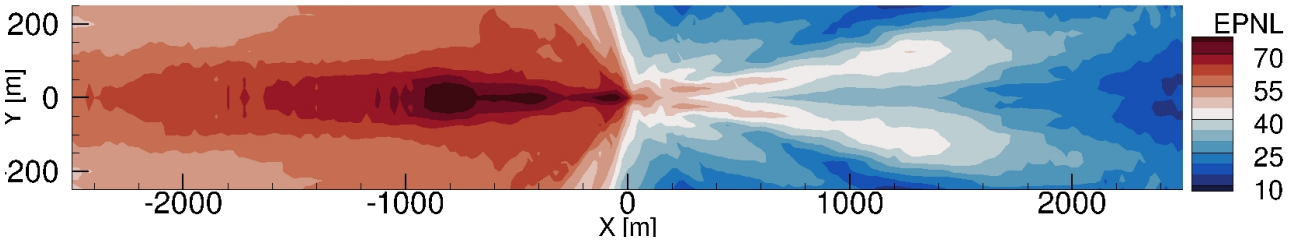

(b) Approach maneuver for minimum time (AT)

Figure 3 – Acoustic footprints in EPNLs of the approach maneuvers

The acoustic footprint due to trajectory DD is characterized by a considerable increase in the spreading of higher noise levels over the flat terrain, rather than being concentrated on either side of the terrain, as depicted in Fig. 4a. This spreading is attributed to the longer flight duration associated with trajectory DD. Additionally, the slightly lower noise levels in the footprint of trajectory DD, as compared to trajectory DT, are ascribed to the slower acceleration achieved during the former, by separate climb and cruise segments. Differently from trajectory DD, the acoustic footprint of trajectory DT is predominantly concentrated on the left half of the domain, mirroring the patterns observed for the approach trajectories. This is attributed to changes in the vehicle pitch attitude angle, which

affects the directivity of noise emissions [5, 7]. Furthermore, the slightly higher noise levels of trajectory DT, as compared to trajectory DD, are attributed to the higher average flight speed over the total duration of the flight.

An interesting pattern is revealed when noise footprints for approach and departure trajectories are compared: considerably lower on-ground noise levels are observed for departure maneuvers than for approach maneuvers. A similar observation has been made in recent work by the authors, where it is found that on-ground noise levels beneath the source increase when the vehicle is pitched up, and conversely, decrease when the vehicle is pitched down [7]. This trend is also confirmed by the present results. Additionally, large lobes of high noise levels are observed around X = -800 meters and Y = 0 meters in the noise footprints of approach trajectories. It is postulated that this trend results not solely from the approach trajectories themselves but from a combination of ground reflection and flight path characteristics, especially given that the lobes are located far from the initial point of both approach trajectories. Both the AD and AT trajectories, which represent landings at different flight speeds, contribute to this phenomenon through strong constructive interference between direct and ground-reflected waves.

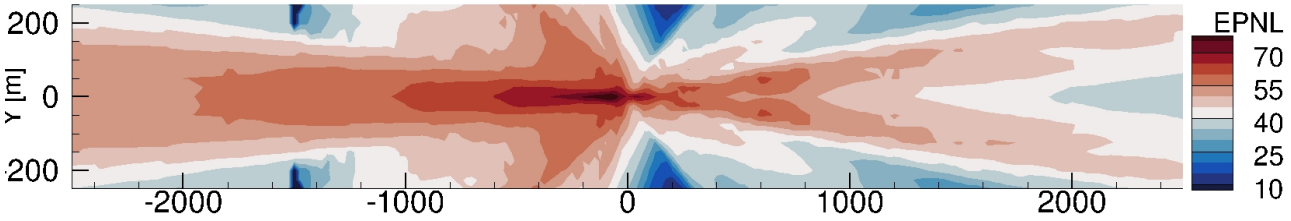

(a) Departure maneuver for minimum distance (DD)

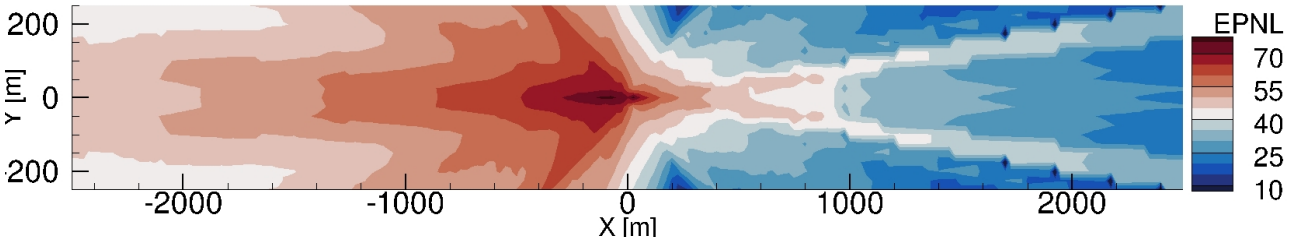

(b) Departure maneuver for minimum time (DT)

Figure 4 – Acoustic footprints in EPNLs of the departure maneuvers

4.3 Perceived Noise Levels

To further investigate the variation of noise levels over the flight duration, time histories of Perceived Noise Levels (PNLs) at several ground Microphone (Mic) locations are examined. PNLs measure the instantaneous loudness of a sound as perceived by a human observer. For this purpose, 5 Mics are considered. Mic 1 and Mic 2 are located on the left part of the terrain, Mic 3 is located over the vertiport center point, while Mic 4 and Mic 5 are located on the right half of the terrain. The microphone coordinates are listed in Table 5.

The computed PNLs over the five Mics are displayed in Fig. 5. Since all trajectories have different duration, for comparison purposes, the flight duration of each trajectory has been normalized by its total duration.

At Mic 1, both approach trajectories start with higher Perceived Noise Levels (PNLs) and then rapidly decrease until 0.15 of the normalized flyover time. After this point, the PNLs of trajectory AT gradually increase, peaking around 0.5 of the normalized flyover time, before gradually decreasing again. The PNLs of trajectory AT exhibit a typical flyover noise time-level history, with the maximum level occurring when the vehicle is directly overhead at Mic 1. Conversely, the trajectory of AD shows an unexpected opposite trend. The exact reason for this behavior is currently under investigation. The Perceived Noise Levels (PNLs) of departure trajectories initially start low and increase rapidly until 0.1 of the normalized flyover time. For the DT trajectory, the PNLs then gradually rise throughout

Table 5 – Coordinates of ground microphones.

	Mic 1	Mic 2	Mic 3	Mic 4	Mic 5
x_E (m)	-150	-50	0	75	175
y_E (m)	0	0	0	0	0
h (m)	1.2	1.2	1.2	1.2	1.2

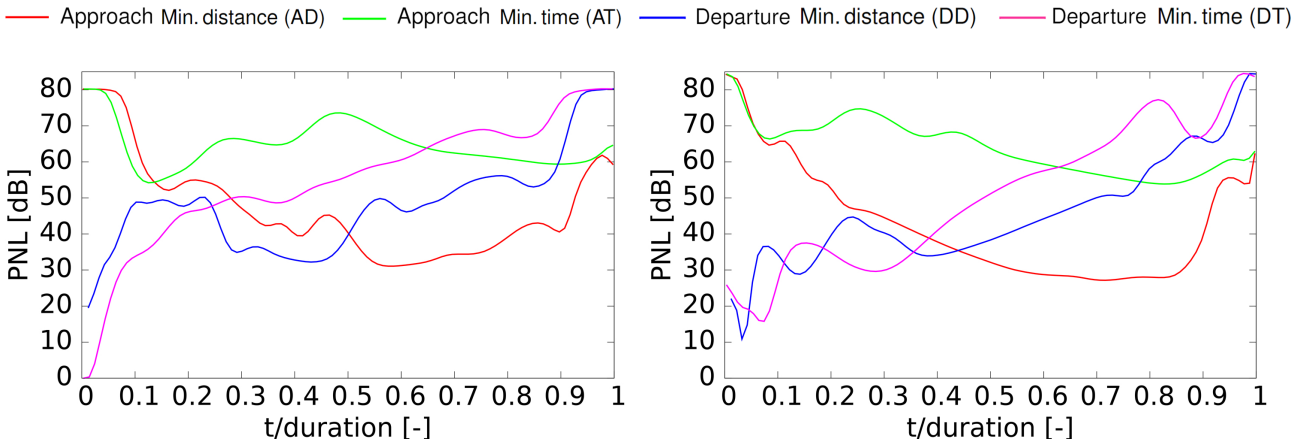

(a) Microphone 1

(b) Microphone 2

(c) Microphone 3

(d) Microphone 4

(e) Microphone 5

Figure 5 – PNLs over the flight duration at the specified ground microphones

the flyover time. In contrast, the PNLs of the DD trajectory remain constant between 0.1 and 0.23 of the normalized flyover time before decreasing until 0.5 of the normalized flyover time, after which they increase gradually. This trend aligns with the flight altitude (h) and flight speed (V) profiles of the departure trajectories shown in Fig. 2b, indicating a high sensitivity of PNLs to flight speed, as PNLs increase with increasing V. Interestingly, until 0.23 of the normalized flyover time, the PNLs of the DD trajectory are higher than those of the DT trajectory. After 0.23, the PNLs of the DD trajectory remain lower than those of the DT trajectory. This pattern is attributed to the source directivity caused by differences in the vehicle's pitch angle at corresponding times. This observation is significant as it highlights the impact of the vehicle's orientation on noise perception. A similar trend was observed in previous work [27].

At Mic 2, a similar trend is observed, with all trajectories starting with slightly higher PNLs. The differences between the PNLs of approach trajectories become increasingly evident over time. PNLs at Mic 3 follow trends similar to those observed at Mics 1 and 2, with the differences between the PNLs of departure trajectories being marginal compared to those of approach trajectories. At Mic 4, a similar trend is noted, except that the PNL of trajectory AT does not remain higher over the flight duration and exhibits a sharper decrease after the vehicle passes over Mic 4. PNLs at Mic 5 show a trend akin to those at Mic 4. It is observed that the PNLs of approach trajectories at the starting point drop by more than 35 dB compared to those at other microphones.

5. Conclusions and future work

For the selected Advanced Air-Mobility quad-rotor flying to/from a vertiport over flat-terrain and in steady atmosphere, minimum-distance approach and departure trajectories are characterized by two clearly distinct phases: one for deceleration from/acceleration to cruise speed at constant altitude, and one for vertical descent/climb at low speed. Minimum-time trajectories are characterized by continuous variation of all flight parameters, with higher speed (on average) throughout the maneuver. For both approach and departure trajectories, the Effective Perceived Noise Levels (EPNLs) of minimum-time trajectories exhibits higher levels and is more concentrated on the left half of the terrain, as compared to the acoustic footprints of minimum-distance trajectories, for which higher EPNLs are more evenly distributed across the entire domain. Acoustic footprints of departure trajectories are lower than those from approach trajectories.

Additionally, the time evolution of PNLs was investigated using five ground microphones. Significant deviations were observed in the PNLs of approach trajectories, except near the starting and terminal points. In contrast, the PNLs of departure trajectories showed very similar temporal patterns. Despite this, both types of trajectories followed the same trend: noise levels were higher for minimum time trajectories compared to minimum distance trajectories.

The obtained results suggest that noise footprints can be considerably reduced by adopting minimum-distance approach/departure trajectories, as they maintain higher distance to the ground for a larger period of time, and approach the ground at lower speed.

5.1 Recommendations

Future work is going to be oriented at increasing the consistency between the low-fidelity flight mechanics model necessary for trajectory optimization, and the models used for aero-acoustic simulation. This can be achieved with the use of optimal surrogate models. Sensitivity studies can be carried out to assess the impact of major operational flight parameters on the acoustic footprint. Future trajectories will have to be simulated over the same spatial domain or time interval to contribute equally to the selected aero-acoustic performance metrics.

6. Contact Author Email Address

C.Varriale@tudelft.nl

7. Copyright Statement

References

[1] H. G. Visser, M. D. Pavel, and S. F. Tang. “Optimization of Rotorcraft Simultaneous Noninterfering Noise Abatement Approach Procedures”. en. In: *Journal of Aircraft* 46.6 (Nov. 2009), pp. 2156–2161. ISSN: 0021-8669, 1533-3868.

[2] T. Tsuchiya et al. “Flight Trajectory Optimization to Minimize Ground Noise in Helicopter Landing Approach”. en. In: *Journal of Guidance, Control, and Dynamics* 32.2 (Mar. 2009), pp. 605–615. ISSN: 0731-5090, 1533-3884.

[3] S. Hartjes. “An Optimal Control Approach to Helicopter Noise and Emissions Abatement Terminal Procedures”. PhD thesis. Delft University of Technology, 2015.

[4] S. Hartjes and H. G. Visser. “Optimal Control Approach to Helicopter Noise Abatement Trajectories in Nonstandard Atmospheric Conditions”. en. In: *Journal of Aircraft* 56.1 (Jan. 2019), pp. 43–52. ISSN: 0021-8669, 1533-3868.

[5] D. Casalino, W. C. van der Velden, and G. Romani. “Community noise of urban air transportation vehicles”. In: *AIAA Scitech 2019 Forum*. 2019, p. 1834.

[6] F. Yunus et al. “Efficient low-fidelity aeroacoustic permanence calculation of propellers”. In: *Aerospace Science and Technology* 123 (2022), p. 107438.

[7] F. Yunus and C. Varriale. “Efficient Noise Footprint Computation for Urban Air Mobility Trajectories in Vertiport Environments”. In: *30th AIAA/CEAS Aeroacoustics Conference (2024)*. American Institute of Aeronautics and Astronautics, May 2024.

[8] W. Johnson. *Rotorcraft Aeromechanics*. Cambridge University Press, Apr. 2013. ISBN: 9781139235655.

[9] D. E. Kirk. *Optimal control theory: an introduction*. Mineola, N.Y: Dover Publications, 2004. ISBN: 978-0-486-43484-1.

[10] D. G. Hull. *Optimal Control Theory for Applications*. Springer New York, 2003. ISBN: 9781475741803.

[11] A. E. Bryson and Y.-C. Ho. *Applied Optimal Control: Optimization, Estimation, and Control*. Routledge, May 2018. ISBN: 9781315137667.

[12] J. T. Betts. *Practical Methods for Optimal Control and Estimation Using Nonlinear Programming, Second Edition*. Second. Society for Industrial and Applied Mathematics, 2010.

[13] A. Wächter and L. T. Biegler. “Line Search Filter Methods for Nonlinear Programming: Motivation and Global Convergence”. In: *SIAM Journal on Optimization* 16.1 (Jan. 2005), pp. 1–31. ISSN: 1095-7189.

[14] A. Wächter and L. T. Biegler. “Line Search Filter Methods for Nonlinear Programming: Local Convergence”. In: *SIAM Journal on Optimization* 16.1 (Jan. 2005), pp. 32–48. ISSN: 1095-7189.

[15] F. Yunus, M. Snellen, and B. von den Hoff. “Predicting tonal noise of full-electric propeller-driven aircraft in outdoor environments using low-order models”. In: *30th AIAA/CEAS Aeroacoustics 2024 Conference*. 2024.

[16] D. Hanson. “Noise radiation of propeller loading sources with angular inflow”. In: *13th Aeroacoustics Conference*. 1990, p. 3955.

[17] D. Hanson. “Sound from a propeller at angle of attack: a new theoretical viewpoint”. In: *Proceedings of the Royal Society of London. Series A: Mathematical and Physical Sciences* 449.1936 (1995), pp. 315–328.

[18] M. T. Kotwicz Herniczek et al. “Evaluation of acoustic frequency methods for the prediction of propeller noise”. In: *AIAA Journal* 57.6 (2019), pp. 2465–2478.

[19] F. Yunus. “Methodologies and algorithms for sound propagation in complex environments with application to urban air mobility: A ray acoustics approach”. Available at https://research.tudelft.nl/en/publications/methodologies-and-algorithms-for-sound-propagation-in-complex-env. PhD thesis. Delft, The Netherlands: Delft University of Technology, Sept. 2023.

[20] F. Yunus et al. “Toward inclusion of atmospheric effects in the aircraft community noise predictions”. In: *The Journal of the Acoustical Society of America* 150.2 (2021), pp. 759–768.

[21] W. Johnson, C. Silva, and E. Solis. *Concept Vehicles for VTOL Air Taxi Operations*. Conference Paper ARC-E-DAA-TN50731. AHS Technical Conference on Aeromechanics Design for Transformative Vertical Flight: NASA Ames Research Center, 2018.

[22] C. Silva et al. “VTOL Urban Air Mobility Concept Vehicles for Technology Development”. In: *2018 Aviation Technology, Integration, and Operations Conference*. American Institute of Aeronautics and Astronautics, June 2018.

[23] F. Yunus et al. “Efficient prediction of urban air mobility noise in a vertiport environment”. In: *Aerospace Science and Technology* 139 (2023), p. 108410.

[24] L. Kiesewetter et al. “A holistic review of the current state of research on aircraft design concepts and consideration for advanced air mobility applications”. In: *Progress in Aerospace Sciences* 142 (Oct. 2023), p. 100949. ISSN: 0376-0421.

[25] D. Casalino et al. “Definition of a benchmark for low Reynolds number propeller aeroacoustics”. In: *Aerospace Science and Technology* 113 (2021), p. 106707.

[26] J. Goldschmidt et al. “Acoustics and Forces from a Subscale Electric Vertical-Takeoff-and-Landing Rotor in Edgewise Flight”. In: *AIAA Journal* (2024), pp. 1–16.

[27] V. T. Valente, E. Greenwood, and E. N. Johnson. “An Experimental Investigation of eVTOL Flight State Variance on Noise”. In: *79th Vertical Flight Society Annual Forum and Technology Display, FORUM 2023*. Vertical Flight Society. 2023.